Wind and Structures, *Vol. 24, No. 4 (2017) 367-384*
DOI: https://doi.org/10.12989/was.2017.24.4.367

Wind tunnel investigation on flutter and buffeting of a three-tower suspension bridge

Wen-ming Zhang[1] and Yao-jun Ge[*2]

[1]*Key Laboratory of Concrete and Prestressed Concrete Structures of the Ministry of Education, Southeast University, 2 Sipailou Road, Nanjing 210096, China*
[2]*State Key Laboratory for Disaster Reduction in Civil Engineering, Tongji University, 1239 Siping Road, Shanghai 200092, China*

(Received November 12, 2015, Revised February 10, 2017, Accepted February 22, 2017)

Abstract. The Maanshan Bridge over Yangtze River in China is a new long-span suspension bridge with double main spans of 2×1080 m and a closed streamline cross-section of single box deck. The flutter and buffeting performances were investigated via wind tunnel tests of a full bridge aeroelastic model at a geometric scale of 1:211. The tests were conducted in both smooth wind and simulated boundary layer wind fields. Emphasis is placed on studying the interference effect of adjacent span via installing a wind deflector and a wind separating board to shelter one span of the bridge model from incoming flow. Issues related to effects of mid-tower stiffness and deck supporting conditions are also discussed. The testing results show that flutter critical wind velocities in smooth flow, with a wind deflector, are remarkably lower than those without. In turbulent wind, torsional and vertical standard deviations for the deck responses at midspan in testing cases without wind deflector are generally less than those at the midspan exposed to wind in testing cases with wind deflector, respectively. When double main spans are exposed to turbulent wind, the existence of either span is a mass damper to the other. Furthermore, both effects of mid-tower stiffness and deck supporting conditions at the middle tower on the flutter and buffeting performances of the Maanshan Bridge are unremarkable.

Keywords: suspension bridge; double main spans; flutter; buffeting; wind tunnel test; full bridge aeroelastic model

1. Introduction

In order to reduce the cost of the foundation and substructures and meet the ever-growing navigational requirements, the multi-span suspension bridge, which has no sharing anchorage, is one of the most favorable and rational solutions for wide and deep straits. There are three long-span suspension bridges with double main spans, i.e., the Taizhou Bridge spanned as 390+2×1080+390 m, the Maanshan Bridge with the span arrangement of 360+2×1080+360 m, and the Yingwuzhou Bridge spanned as 225+2×850+225 m, over the Yangtze River in China. The Chacao Channel suspension bridge with double main spans of 1055+1100 m, which was abolished by the Chile government due to

*Corresponding author, Professor, E-mail: yaojunge@tongji.edu.cn

http://www.techno-press.com/journals/was&subpage=7 ISSN: 1226-6116 (Print), 1598-6225 (Online)

economic reasons in 2006, has been restarted recently.

Before reaching the top of the middle pylon, main cables of a double-main-span suspension bridge go over side pylons and a main span from both anchors (Ge and Xiang 2011). In comparison to the common suspension bridges with single main span, due to the lack of effective longitudinal restraint of the middle pylon, the double-main-span suspension bridge becomes a structural system with greater flexibility, and is more susceptible to wind action (Zhang 2010). Researches mainly focus on wind-resistant performance of the traditional suspension bridges with single main span (Boonyapinyo *et al*. 2006, Chen *et al*. 2001, Davenport 1962, Ge and Tanaka 2000, Katsuchi *et al*. 1999, Lin 1979, Thorbek and Hansen 1998, Xu *et al*. 2000, Scanlan and Gade 1997), but only a few studies on flutter and buffeting performances of multiple-main-span suspension bridges have been conducted to date. Larsen (2003) reported aerodynamic information of a 1:215 scale full aeroelastic model for the above-mentioned Chacao Bridge in both smooth and turbulent flow. In Yamada and Katsuchi (2005), flutter characteristics of a four-span suspension bridge with main spans of 2000-4000 m were investigated numerically. In Yoshida *et al*. (2004), the flutter critical wind velocity of a four-span suspension bridge with two main spans of 2000m was calculated using the Selberg formula. Zhang (2008, 2010) examined flutter and structural parameters on flutter of the aforementioned Taizhou Bridge numerically.

Either span of a double-main-span suspension bridge is not an independent structure, because energy delivers between two main spans through main cables and deck in wind induced vibrations. In flutter or buffeting, deck vibrations in two adjacent spans may interfere or influence each other, which can be defined as interference effect of adjacent span. When span A vibrates, may the adjacent span B act as a vibration exciter or mass damper of span A? It is hoped that this interesting question will be resolved in this paper by comparing the vibration response of span A in two different testing cases: span B is sheltered from wind, and exposed to wind. Research on interference effect of adjacent span is helpful to understand flutter oscillation modes and mechanism, and will also provide reference for finding out the qualitative and/or quantitative relationship between the wind-resistant performances of multiple-main-span suspension bridges and traditional single-main-span suspension bridges, which is very helpful in making it convenient for engineers to estimate wind-resistant performances of multiple-main-span suspension bridges in preliminary design phase according to those of traditional single-main-span suspension bridges.

In wind tunnel tests of the aeroelastic full-bridge model for the Maanshan Bridge, which is taken as an engineering example in this paper, interference effect of adjacent span is studied via installing a wind deflector and wind separating board in wind tunnel to shelter one span of the bridge model from incoming flow. Furthermore, combined effects of the wind deflector, the stiffness of the mid-tower and the supporting conditions of the deck on flutter and buffeting performances of suspension bridges are discussed.

2. Maanshan Bridge project

The Maanshan Bridge over the Yangtze River is spanned as 360+2×1080+360 m (Fig. 1) with three 176 m high pylons of frame-structure. Its deck of closed streamline cross-section of single steel box with two wind-fairings is 38.5 m wide and 3.5 m high (Fig. 2). The lower crossbeam of the middle pylon is through the deck, making the deck fixed to the middle pylon. This bridge is described in detail by Zhang *et al*. (2011).

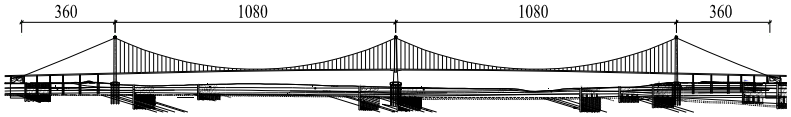

Fig. 1 Elevation of the Maanshan Bridge (unit: m)

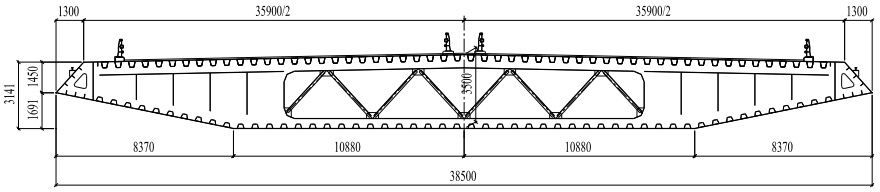

Fig. 2 Deck cross-section (unit: mm)

According to the observation data, the exponent of mean wind profile at the bridge site is about 0.12, and the basic wind speed at the bridge site (U_{10}), namely the yearly-maximum 10-min averaged mean wind speed at 10 m height corresponding to 100-year return period, is 31.8 m/s. Thus, the design reference wind speed (U_d) at deck level (57.8 m above normal water level) is as follows

$$U_d=U_{10}(57.8/10)^{0.12}=39.3\text{m/s} \tag{1}$$

The flutter checking wind speed can then be obtained as follows

$$[U_{cr}]=K\mu_f U_d=56.6\text{m/s} \tag{2}$$

where μ_f is a synthetic coefficient considering the influence of turbulence on wind speed and the incomplete correlation of winds along the bridge span. It depends on the local terrain condition and the length of bridge span, and is set to 1.2 here according to the literature (Xiang *et al*. 1996); K is a comprehensive safety factor, considering the uncertainties in wind tunnel test, design and construction of bridge, and is set to 1.2 according to the literature (Xiang *et al*. 1996).

3. Aeroelastic full-bridge model

The aeroelastic full-bridge model test was carried out in the TJ-3 Wind Tunnel of the State Key Laboratory for Disaster Reduction in Civil Engineering at Tongji University, China. The wind tunnel is a large boundary layer wind tunnel with a closed testing section of 15 m width, 2 m height and 14 m length. The achievable mean wind speed of empty wind tunnel ranges from 1.0 to 17.6 m/s, adjustable continuously (Zhu *et al*. 2007).

3.1 Model design and manufacture

Based on the prototype structure and the overall principles of aeroelastic model design, the model with a geometric scale of 1:211 was designed and constructed. The scale of 1:211 was chosen to obtain a full utilization of the width of the wind tunnel (15 m) and also gain the

convenience of finding a kind of high tensile steel wire with very suitable axial stiffness to simulate main cables. This scale results in a velocity scale of 1: 14.53 and a frequency scale of 14.53:1 (Ge and Zhou 2008). The main physical parameters are given in Table 1.

The deck model was comprised of a steel core beam (simulating the deck stiffness), high-dense foam coats (simulating the deck appearance) and lead compensating weights. The compensating weights were installed in the foam coats to adjust the mass and mass moment of inertia of the

Table 1 Physical parameters of the full bridge aeroelastic model

Parameters		Unit	Prototype	Scaling	Model
Length (L)		m	360+2×1080+360	λ_L=1:211	1.706+2×5.118+1.706
Width (B)		m	38.5	λ_L=1:211	0.182
Depth (H)		m	3.5	λ_L=1:211	0.017
Mass (m)	Deck	kg/m	2.029×10^4	λ_m=1:211^2	0.455
	Main cables	kg/m	2.403×10^3	λ_m=1:211^2	0.054
Mass moment of deck (J_m)		kg·m^2/m	2.360×10^6	λ_{Jm}=1:211^4	0.0012
Stiffness of deck	Vertical (EI_V)	N·m^2	6.474×10^{11}	λ_{EI}=1:211^5	1.55
	Lateral (EI_L)	N·m^2	4.162×10^{13}	λ_{EI}=1:211^5	99.5
	Torsional (GJ)	N·m^2	1.829×10^{12}	λ_{GJ}=1:211^5	4.37
Stiffness of main cables (EA)		N	5.982×10^{10}	λ_{EA}=1:211^3	6370
Frequency(f)	A-V-1	Hz	0.0843	λ_f=$211^{1/2}$:1	1.2240
	S-V-1	Hz	0.1169	λ_f=$211^{1/2}$:1	1.7003
	A-L-1	Hz	0.0947	λ_f=$211^{1/2}$:1	1.3749
	S-L-1	Hz	0.0962	λ_f=$211^{1/2}$:1	1.3967
	A-T-1	Hz	0.2675	λ_f=$211^{1/2}$:1	4.0326
	S-T-1	Hz	0.3386	λ_f=$211^{1/2}$:1	4.9189
Structural Damping (ξ)		—	0.005	λ_ξ=1:1	0.005
Maximum Testing Speed (U)		m/s	120	λ_v=1:$211^{1/2}$	8.25

Fig. 3 Full bridge aeroelastic model in TJ-3 wind tunnel

deck. The measured mass and mass moment of inertia of the model deck are 0.431 kg/m and 0.00114 kg·m^2/m, respectively, and both are very close to their target values as listed in Table 1. The foam coats were connected to the core beam with steel transverse bars. Similarly, the models of the bridge pylons were composed of steel frames, perspex coats and copper compensating weights. The two main suspension cables were modeled by two high-strength steel wires with equivalent axial stiffness and fitted with lead circular cylinders to provide the necessary mass and aerodynamic drag. The hangers were made of constantan wires, and the deficient mass of each hanger was compensated in deck and main cables at 1:1 ratio, because the local vibration of hangers was not a research content of this study. The full aeroelastic model in the wind tunnel is shown in Fig. 3.

3.2 Arrangement of measuring points

According to computed mode shapes of the Maanshan Bridge (Zhang *et al*. 2011), six deck sections (Fig. 4), i.e., midspan, quarter-span near middle tower and quarter-span near side tower of every main span, were selected to arrange measuring points. For all three sections of span A and the midspan section of span B, three laser displacement meters were installed on each section. Two of them are for vertical displacement response, while the other one is for lateral. Three accelerometers were installed on the quarter-span section near middle tower and the one near side tower, respectively, at span B. Similarly, two of them are for vertical acceleration response, while the other one is for lateral.

3.3 Modal check of the aeroelastic model

Natural frequencies of all three aeroelastic tower models in free-standing configuration were firstly tested using free-decay vibration approach before they were assembled into the aeroelastic full-bridge model. Results are compared with the target values in Table 2. A good agreement can then be found between the measured and target frequencies.

To ensure the accuracy of simulating the bridge dynamic properties, the modal parameters of the full-bridge model, including natural frequencies, modal damping ratios and mode shapes of the model were carefully checked after it was manufactured.

As shown in Table 3, the frequencies and modal damping ratios were identified with conventional approach of free decay vibration stimulated with initial displacement for lower frequency modes or with initial impulse for higher frequency modes. Computed frequencies of

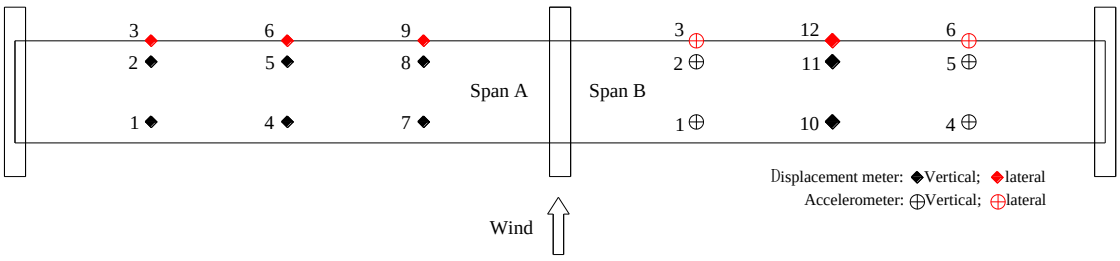

Fig. 4 Measuring points on the deck of model

Table 2 Natural frequencies of prototype and model for towers in free-standing configuration

Modes	Side towers						Middle tower			
	Computed values of prototype (Hz)	Target values of model (Hz)	Span A		Span B		Computed values of prototype (Hz)	Target values of model (Hz)	Measured values (Hz)	Discrepancy (%)
			Measured values (Hz)	Discrepancy (%)	Measured values (Hz)	Discrepancy (%)				
Longitudinal bending	0.153	2.220	2.250	1.35	2.188	-1.44	0.295	4.307	4.199	1.40
Lateral bending	0.252	3.670	3.790	3.27	3.750	2.18	0.362	5.354	5.371	-2.50
Torsional	0.631	9.171	9.030	-1.54	9.375	2.22	0.870	12.713	12.891	0.32

Table 3 Modal parameters of prototype and model for full-bridge

Modes	Computed frequencies of prototype (Hz)	Frequencies of model (Hz)			Measured damping ratios of model (%)
		Target values	Measured values	Discrepancy (%)	
A-V-1	0.0843	1.224	1.270	3.8	0.30
A-L-1	0.0947	1.375	1.367	-0.6	0.92
S-L-1	0.0962	1.397	1.465	4.9	3.52
A-T-1	0.2675	4.033	4.297	6.5	0.45
S-T-1	0.3386	4.919	4.883	-0.7	0.48

Note: S–symmetric, A–anti-symmetric, V–vertical, L–lateral, T–torsional

prototype (Zhang *et al*. 2011) and the target frequencies of model are also listed in Table 3. From Table 3, one can find that the frequency discrepancies are less than 5% except for that of the mode A-T-1, which reaches 6.5%. Furthermore, the modal damping ratios of the vertical and torsional modes were about 0.5%, which were close to that suggested in Xiang *et al*. (1996) for steel bridges.

In order to check the distribution of stiffness and mass for the deck of model, an ambient vibration approach using turbulent wind with lower speed of 1 m/s as a major source of the ambient excitation was employed to measure the mode shapes of the full-bridge model. It is necessary to firstly get natural frequencies by analyzing the relationship of the coherency function and phase between each measuring point. Mode shapes can then be indentified through calculating the ratio of auto-power spectrum amplitude at corresponding natural frequency of every measuring

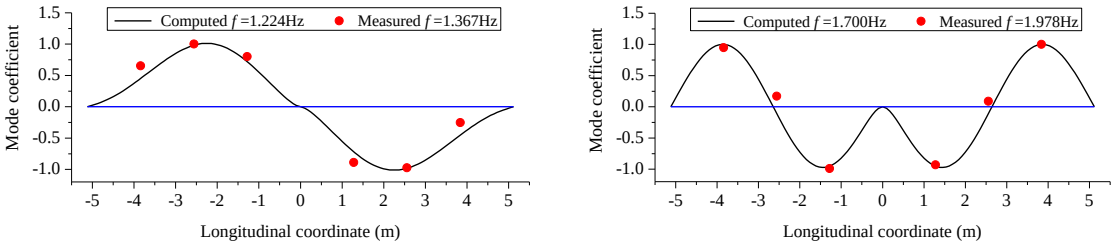

(a) A-V-1 mode (b) S-V-1 mode

Fig. 5 Computed and measured vertical mode shapes

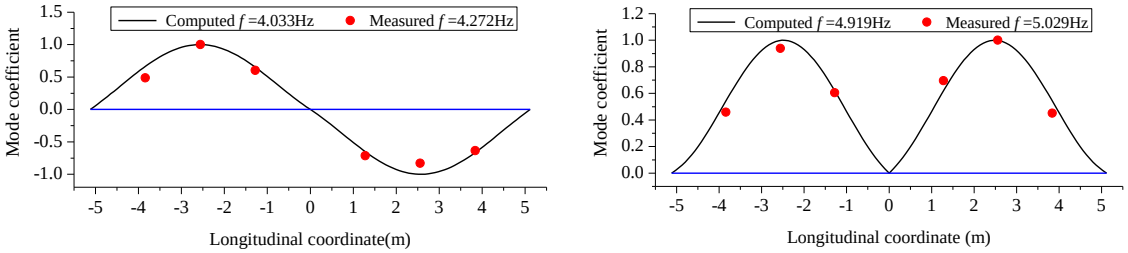

(a) A-T-1 mode (b) S-T-1 mode

Fig. 6 Computed and measured torsional mode shapes

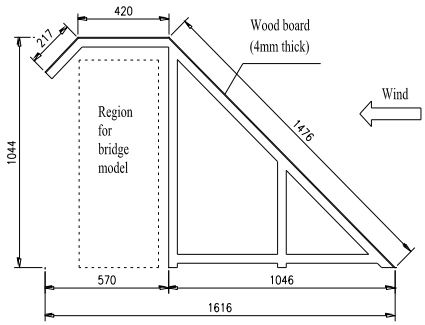

Fig. 7 Cross section of wind deflector (unit:mm)

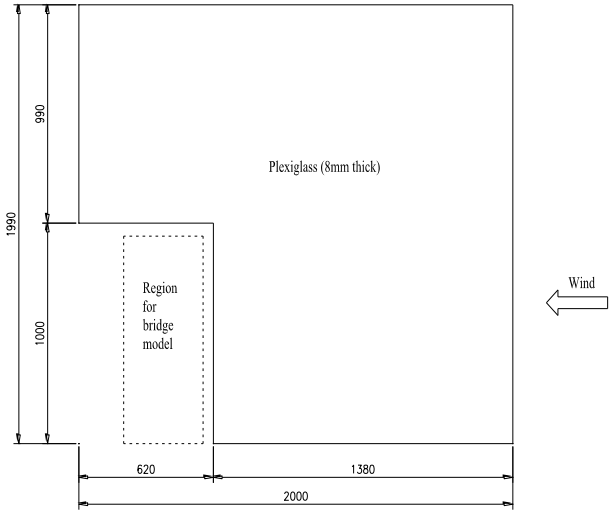

Fig. 8 Wind separating board (unit:mm)

point. The identified vertical bending and torsional mode shapes are shown in Figs. 5 and 6, respectively, together with those computed using ANSYS. It is found from these figures that the discrepancies between the measured and computed mode shapes are insignificant.

4. Wind deflector and wind separating board

As shown in Fig. 7, the wind deflector, made of wood board, is a little higher than the tower of bridge model. The total length of the wind deflector is 7.5 m, which is one half of the wind tunnel width. Span B of the bridge model will be sheltered from incoming wind flow if the wind deflector is installed. To avoid the air disturbance induced by the end of the wind deflector near the middle tower, a wind separating board was glued to the end of the wind deflector. The wind separating board, made of plexiglass and reinforced by aluminium squares, is 1.99 m high (Fig. 8) and its top is very close to the ceiling of the wind tunnel. The length and thickness of the wind separating board are 2 m and 0.008 m, respectively. As a result, the wind tunnel will be divided into two if the

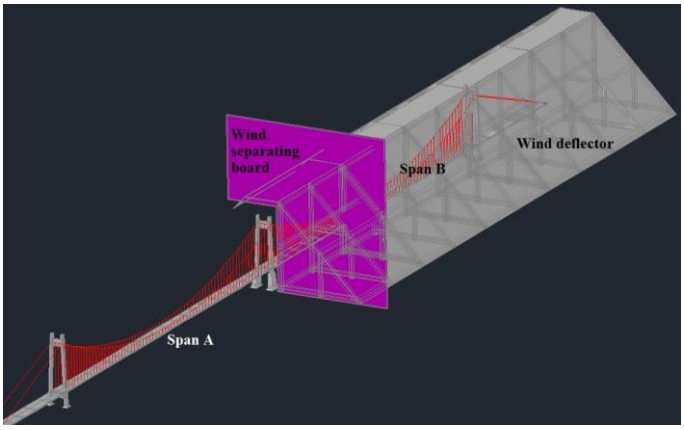

Fig. 9 Arrangement of the wind deflector, wind separating board and bridge model

Fig. 10 Wind deflector, wind separating board and bridge model in wind tunnel

wind separating board is installed. The arrangement of the wind deflector, wind separating board and bridge model is shown in Figs. 9 and 10. In testing cases without wind deflector, both span A and span B are exposed to incoming wind flow. However, only span A is exposed to incoming wind flow in testing cases with wind deflector.

5. Wind flow simulation

The atmospheric boundary layer was simulated in the TJ-3 wind tunnel using roughness elements and spirelets. The simulated profiles of mean wind, alongwind and vertical turbulent intensities are shown in Figs. 11-13, where the gradient height (z_g) is taken as 300 m for the terrain of type A (α=0.12). The measured alongwind and vertical turbulent intensities near deck level in the wind tunnel (z=0.274 m, z/z_g=0.194) were about 11.5% and 6.7%, respectively. The measured spectra of turbulence at this level, together with some empirical spectra are shown in Figs. 14.

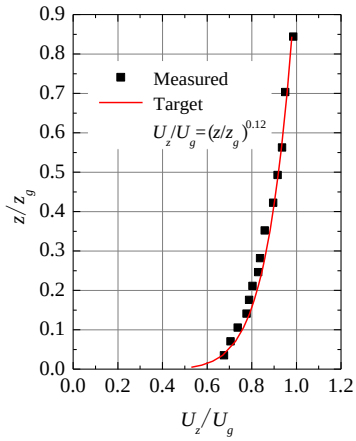

Fig. 11 Profile of mean wind speed

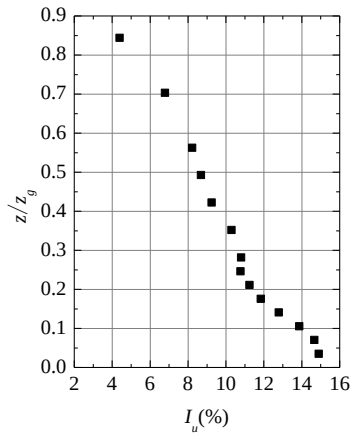

Fig. 12 Profile of alongwind turbulent intensity

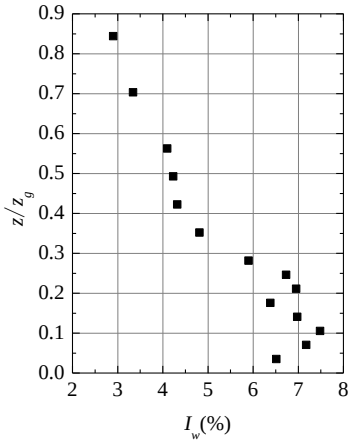

Fig. 13 Profile of vertical turbulent intensity

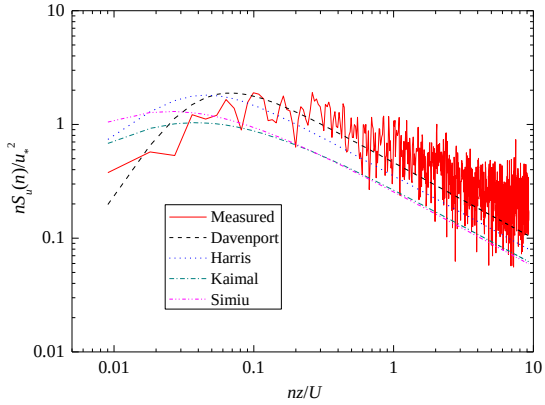

(a) alongwind component *u*

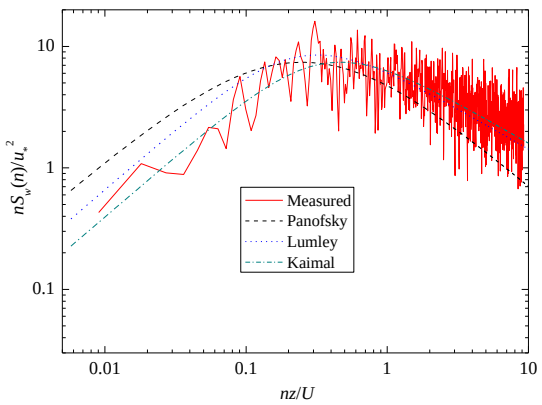

(b) vertical component *w*

Fig. 14 Spectrum of turbulence at deck level

6. Experimental procedure

The preceding full aeroelastic model is original and corresponds to the prototype, in which the deck was fixed to the middle tower. In other words, the deck was supported by solid joint at the middle tower. After several test cases were conducted using this model, the connection between the deck and the middle tower was changed into hinge joint, in which just three degrees of freedom, i.e., vertical, lateral and rotation about the longitudinal bridge axis, of the deck were coupled with the middle tower. Aim for this change is to research effect of supporting condition under the deck on the flutter and buffeting performances of a double-main-span suspension bridge.

In order to study the effect of middle tower stiffness on the flutter and buffeting performances, the middle tower containing two columns was remodeled with infinite stiffness in a simple way. The top of each column was tied to the floor by four wires in different directions, making three degrees of freedom, i.e., longitudinal, transverse and rotation about the vertical axis, of the tower

Table 4 Numbers of testing cases

Wind field	Wind inclination angle (θ)	Deck is supported by solid joint at mid-tower				Deck is supported by hinge joint at mid-tower			
		Mid-tower top is free		Mid-tower top is fixed		Mid-tower top is free		Mid-tower top is fixed	
		w/o WD*	w/ WD	w/o WD	w/ WD	w/o WD	w/ WD	w/o WD	w/ WD
Smooth	-3°	S-1	S-2	S-3	S-4	S-5	S-6	S-7	S-8
	0°	S-9	S-10	S-11	S-12	S-13	S-14	S-15	S-16
	+3°	S-17	S-18	S-19	S-20	S-21	S-22	S-23	S-24
Turbulent	0°	T-1	T-2	T-3	T-4	T-5	T-6	T-7	T-8

*Note: WD = wind deflector

top constrained. This constraint condition of the middle tower will be called "mid-tower top is fixed" in the following discussion. By the way, the original configuration of the middle tower before this change will be called "mid-tower top is free" in the following discussion.

The tests were carried out in both smooth wind field ('smooth wind' for short) and simulated turbulent wind field of boundary layer mentioned above ('turbulent wind' for short). In the turbulent-wind tests, only one wind inclination angle (θ), θ=0°, was considered. For the smooth-wind test, three inclination angles (θ), θ=-3°, 0°, 3° , were taken into account.

In summary, test cases were the combinations of the supporting condition of the deck at the middle tower, the stiffness of the middle tower, installing wind deflector or not, and wind inclination angle. As listed in Table 4, totally 24 and 8 combinations were considered in smooth wind and turbulent wind, respectively.

7. Major test results of flutter

In smooth flow, coupled flutter instability did exist. Critical wind speeds were collected and listed in Table 5, where, wind speeds have been transferred to the prototype values. The wind speed beyond which the peak factor of deck vibration is less than or equal to 2.0 was taken as the threshold. As can be seen from column (2) in Table 5, flutter critical wind speeds of the Maanshan Bridge are much greater than the flutter checking wind speed 56.6 m/s, demonstrating that the

Table 5 Flutter critical wind speeds in smooth flow (m/s)

Wind inclination angle (θ)	Deck is supported by solid joint at mid-tower				Deck is supported by hinge joint at mid-tower			
	Mid-tower top is free		Mid-tower top is fixed		Mid-tower top is free		Mid-tower top is fixed	
	w/o WD*	w/ WD	w/o WD	w/ WD	w/o WD	w/ WD	w/o WD	w/ WD
(1)	(2)	(3)	(4)	(5)	(6)	(7)	(8)	(9)
-3°	79.9	64.0	78.5	65.5	84.4	66.9	81.5	71.3
0°	90.2	64.0	85.1	69.8	90.2	74.2	89.3	74.2
+3°	74.2	55.3	74.2	59.6	65.5	52.4	69.8	58.1

*Note: WD=wind deflector

Maanshan Bridge has enough aerodynamic stability in smooth wind field. Flutter oscillation, however, did not arise in turbulent flow up to the wind speed of 85m/s, beyond which the aeroelastic model stochastically vibrated with large amplitudes in vertical bending but not related to any aerodynamic instability.

7.1 Interference effect of adjacent span

When comparing column (2) with (3), (4) with (5), (6) with (7), (8) with (9) in Table 5, respectively, one can find that flutter critical wind velocities in smooth flow, with a wind deflector, are remarkably lower than those without. The flutter dominant modes, with wind deflector and without, are the first anti-symmetric torsional mode (A-T-1) and the first symmetric torsional mode (S-T-1), respectively. The natural frequency of mode A-T-1 is lower than that of mode S-T-1 (Zhang *et al*. 2011). By the way, mode A-T-1 and S-T-1 are the first and second torsional mode, respectively, in the natural mode list of the Maanshan Bridge.

Case S-4 can be taken as an illustrative example for the testing cases with wind deflector. Testing curves of the torsional and vertical standard deviations (σ_{Tor}, σ_{Ver}) vs. mean wind speed (U), for the deck response at midspan in smooth wind are illustrated in Fig. 15, where, the responses and wind speed have been transferred to the prototype values. The reference wind speed was measured at deck level in wind tunnel. As observed from Fig. 15, torsional and vertical standard deviations of span A are greater than those of span B, respectively. Furthermore, the slope of every response curve with wind speed increases remarkably when wind speed exceeds the flutter threshold. Torsional responses of deck midspans at U=65.5 m/s are shown in Fig. 16. As can be seen from Fig. 16, the vibrating phase of span A is nearly opposite of span B, meaning that the dominant mode of flutter is mode A-T-1.

As for case S-9 and S-10, aerodynamic flutter was investigated numerically by full-mode aerodynamic flutter analysis (Zhang *et al*. 2011). Flutter derivatives used in the analysis were obtained from sectional model test (Ge and Zhou 2008). The variations of the damping ratios of traced modes, A-T-1 and S-T-1, versus wind velocity are shown in Fig. 17.

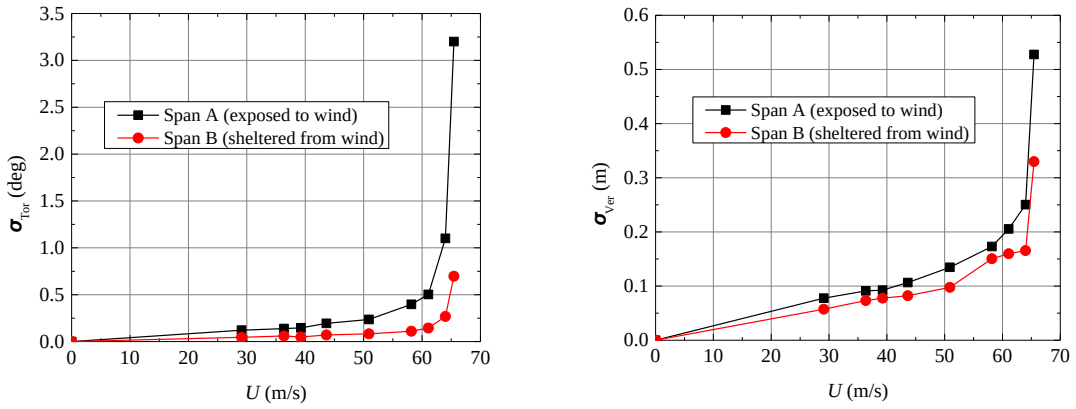

(a) torsional (b) vertical

Fig. 15 Standard deviations of responses to smooth wind at deck midspans (case S-4)

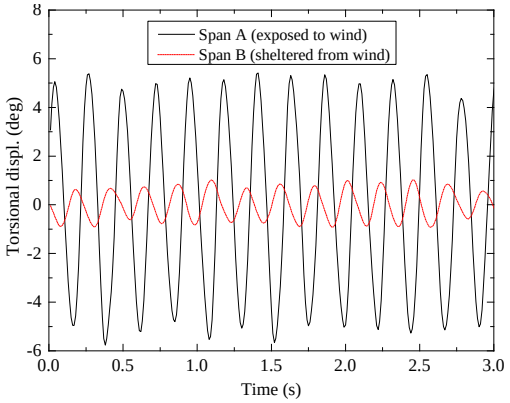

Fig. 16 Torsional responses at deck midspans (case S-4, U=65.5 m/s)

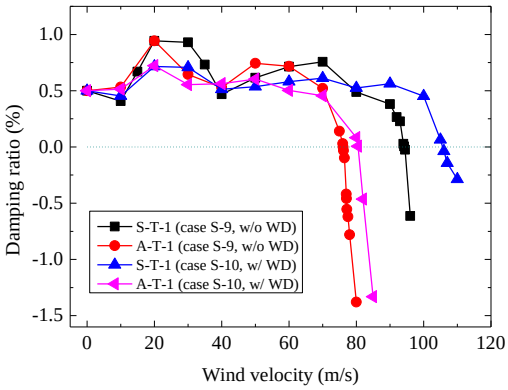

Fig. 17 Variation of damping ratio versus wind velocity

As observed from Fig. 17, in the case without wind deflector, flutter critical wind speed of mode A-T-1 (76.1 m/s) is less than that of mode S-T-1 (94.5 m/s). Therefore, flutter dominant mode should be mode A-T-1 in this case. However, a unique flutter-mode transition behavior was observed in smooth flow. As wind speed approaches the flutter threshold, the model oscillation with mode A-T-1 transfers to alternate torsional oscillation between double spans, then transfers to oscillation with the mode S-T-1, and violent oscillation occurs at last (Zhang and Ge 2014). As a result, the flutter dominant mode is mode S-T-1. By the way, this flutter-mode transition behavior didn't occur in the testing cases with wind deflector, in which the flutter dominant mode is mode A-T-1.

As also can be seen from Fig. 17, flutter critical wind speed of mode A-T-1 (76.1 m/s), without wind deflector, is less than that (80.5 m/s) with, and so is mode S-T-1. However, flutter critical wind speed of mode A-T-1 (80.5 m/s), with wind deflector, is still less than that of mode S-T-1 (94.5 m/s) without, proving that the wind deflector can't increase the flutter critical wind speed of the Maanshan Bridge.

7.2 Effect of mid-tower stiffness

When comparing column (2) with (4), (3) with (5), (6) with (8), (7) with (9) in Table 5, respectively, one can find that flutter critical wind speeds with free mid-tower top are almost same as those with fixed mid-tower top. It is indicated that middle tower stiffness has little effect on flutter performance of the Maanshan Bridge.

7.3 Effect of deck supporting condition

When comparing column (2) with (6), (3) with (7), (4) with (8), (5) with (9) in Table 5, respectively, one can find that flutter critical wind speeds with solid joint are almost same as those with hinge joint. It is meant that supporting condition of the deck at the middle tower also has little effect on flutter performance of the Maanshan Bridge.

8. Major test results of buffeting

8.1 Interference effect of adjacent span

The test curves of the torsional and vertical standard deviations (σ_{Tor}, σ_{Ver}) vs. mean wind speed (U), for the deck responses at two midspans, to turbulent wind are shown in Figs. 18-21, where, the responses and wind speed have also been transferred to the prototype values.

As can be seen from these figures, torsional and vertical standard deviations for span A, without wind deflector, are generally less than those with, respectively. It is indicated that, when double main spans of the Maanshan Bridge are exposed to wind, the existence of either span is a mass damper to the other. The reason is discussed as follows. The lift coefficient of aerostatic force for the deck at θ=0° is minus in value (Zhang *et al*. 2013), and thus the lift force acting on the deck is downwards. As a result, the sag effect of main cables decreases, and the structural gravity stiffness increases. Accordingly, the structural overall tangent stiffness increases. In testing cases with wind deflector and without, the downwards lift force of the deck acts on only one span and double spans, respectively. The structural gravity stiffness, without wind deflector, is greater than that with.

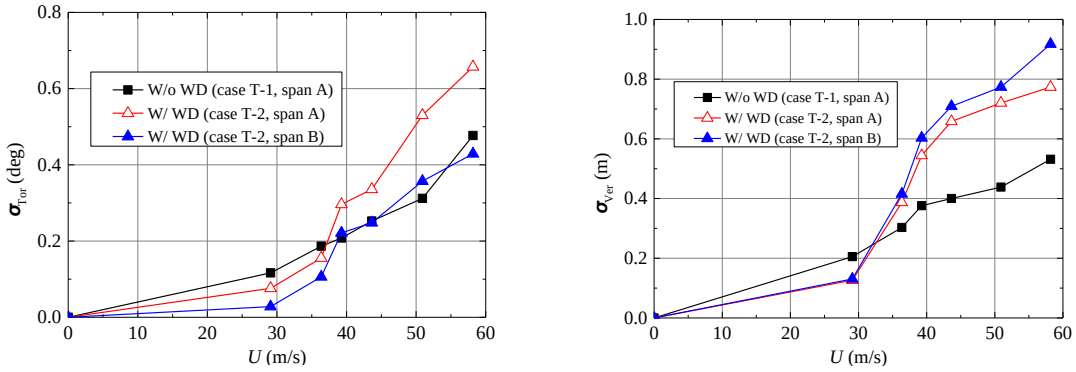

(a) torsional (b) vertical

Fig. 18 Standard deviations of buffeting responses at deck midspans (case T-1 and T-2)

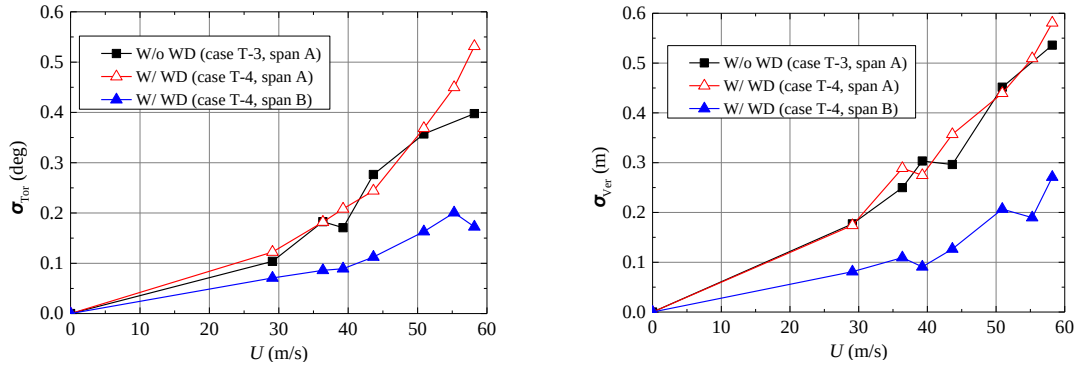

(a) torsional (b) vertical

Fig. 19 Standard deviations of buffeting responses at deck midspans (case T-3 and T-4)

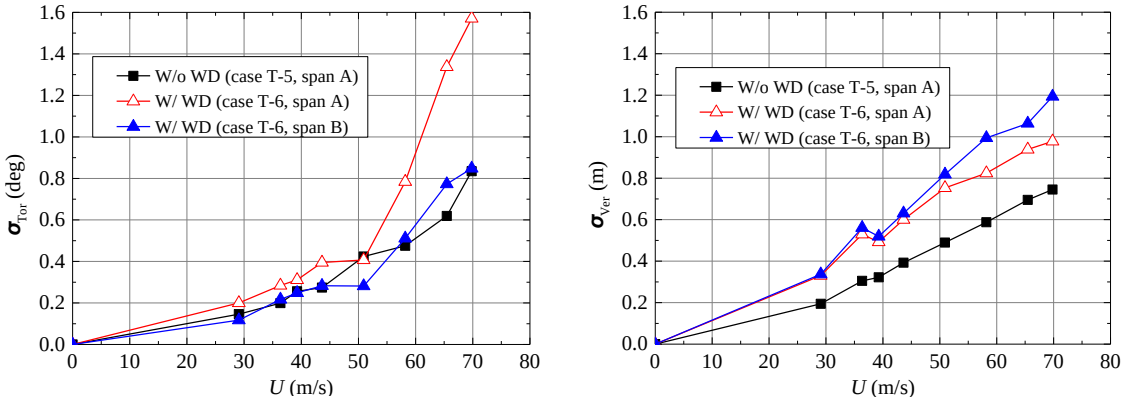

(a) torsional (b) vertical

Fig. 20 Standard deviations of buffeting responses at deck midspans (case T-5 and T-6)

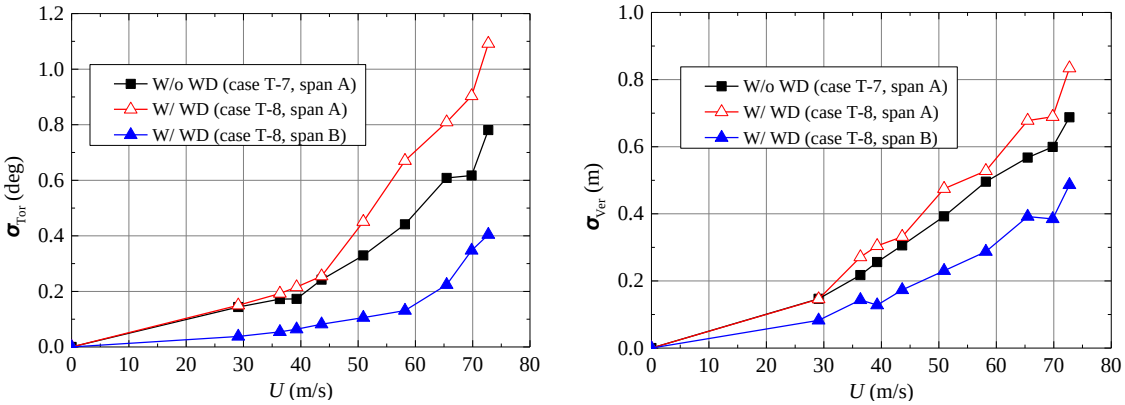

(a) torsional (b) vertical

Fig. 21 Standard deviations of buffeting responses at deck midspans (case T-7 and T-8)

As also shown in Figs. 18-21, in testing cases with wind deflector, the torsional standard deviations for span A, exposed to wind, are much greater than those for span B, sheltered from wind, and the difference between them has a tendency to increase with the increasing wind speed.

From Fig. 18(b) and Fig. 20(b) one can find that, in testing cases with wind deflector, the vertical standard deviations for span A, exposed to wind, are slightly less than those for span B, sheltered from wind, when mid-tower top is free. When mid-tower top is fixed, concludes are opposite, as shown in Fig. 19(b) and Fig. 21(b).

In testing cases with wind deflector, span A is motivated by incoming flow directly, and absorb energy from wind constantly. Span B, however, can't get energy from wind directly, and thus the vibration energy is completely delivered from span A.

When mid-tower top is free, span A has two ways to deliver energy to span B. One way is across suspenders, main cables of span A, vibrating middle tower, main cables and suspenders of span B before energy reaches the deck of span B. The other way is through deck directly. In spite of this, span B can't, after all, absorb energy from wind directly. Torsional and vertical responses of span B, therefore, should be less than those of span A. However, downwards lift force acting on

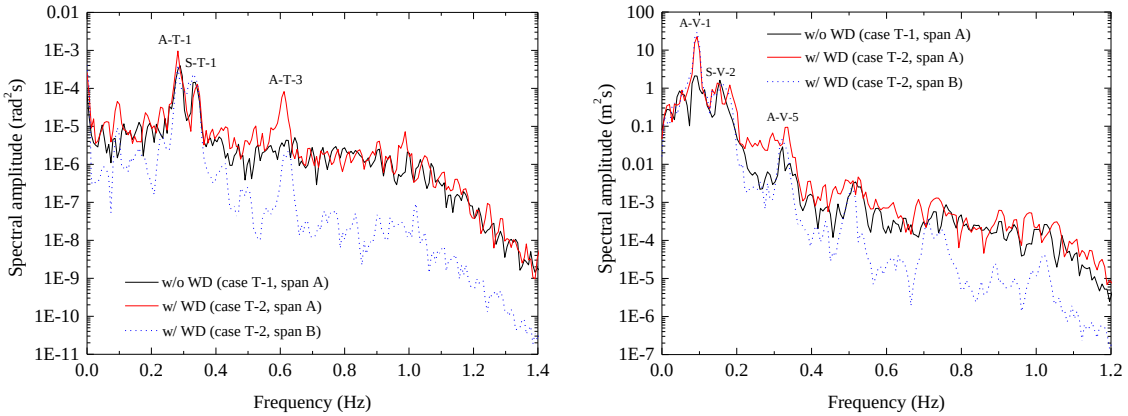

(a) torsional (b) vertical

Fig. 22 Spectra of buffeting responses at deck midspans (case T-1 and T-2, U=39.3 m/s)

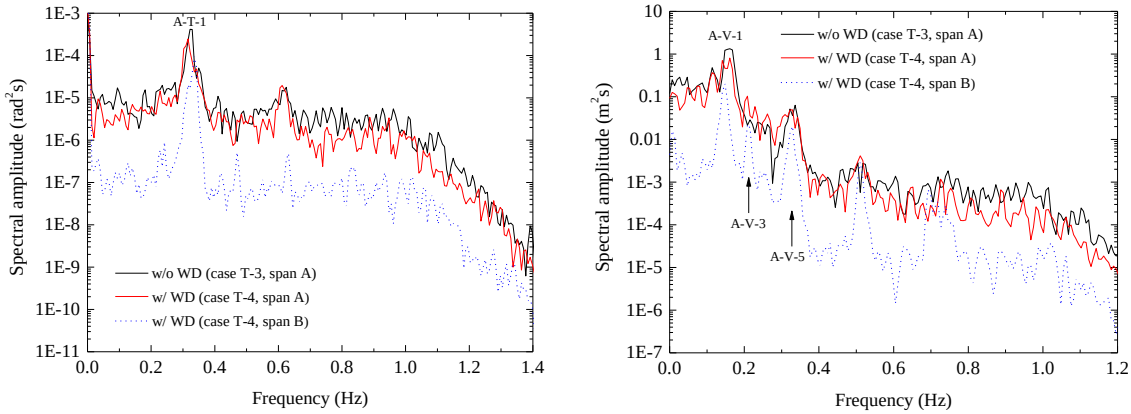

(a) torsional (b) vertical

Fig. 23 Spectra of buffeting responses at deck midspans (case T-3 and T-4, U=39.3 m/s)

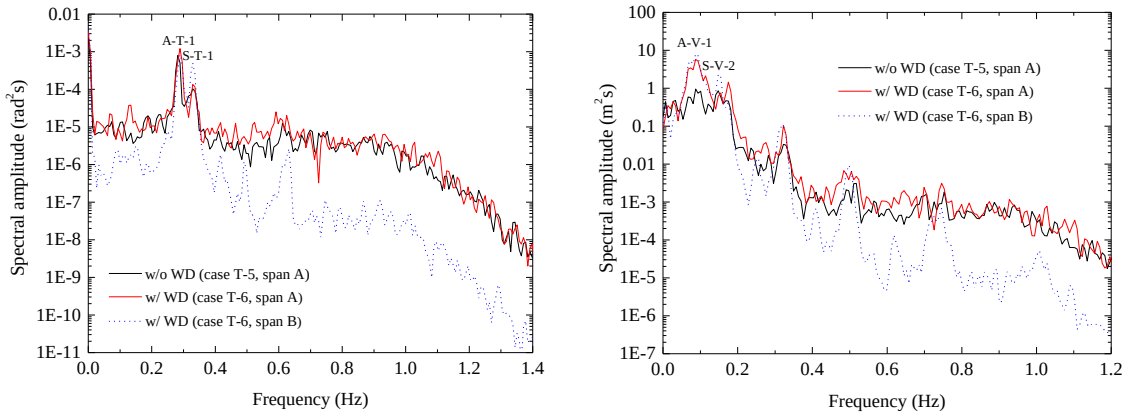

(a) torsional (b) vertical

Fig. 24 Spectra of buffeting responses at deck midspans (case T-5 and T-6, U=39.3 m/s)

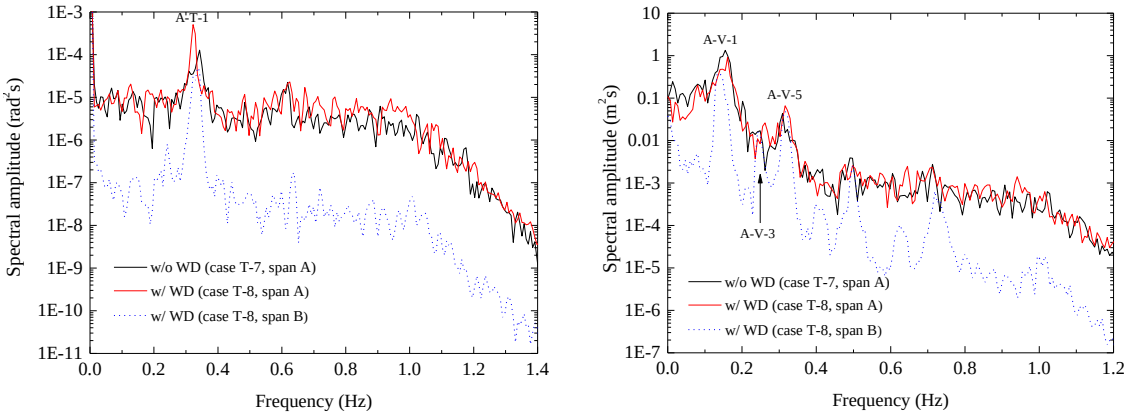

(a) torsional (b) vertical

Fig. 25 Spectra of buffeting responses at deck midspans (case T-7 and T-8, U=39.3 m/s)

deck increases the structural gravity stiffness of span A, which affects vertical bending stiffness of deck directly. That's the reason why the vertical responses of span A are slightly less than those of span B. On the other hand, torsional stiffness of deck is affected by the structural gravity stiffness indirectly, and thus is less sensitive to aerostatic load than vertical bending stiffness. That's the reason why the torsional responses of span A are still greater than those of span B.

From the response spectra, as shown in Figs. 22-25, one can see that the fundamental modes of deck vertical bending, and torsional vibrations provided the major contributions to the buffeting responses, although several higher modes also exerted a little effect on the responses. It is noteworthy that resonant component is dominant in the buffeting response, and the contribution of the background component is very small.

8.2 Effect of mid-tower stiffness and deck supporting condition

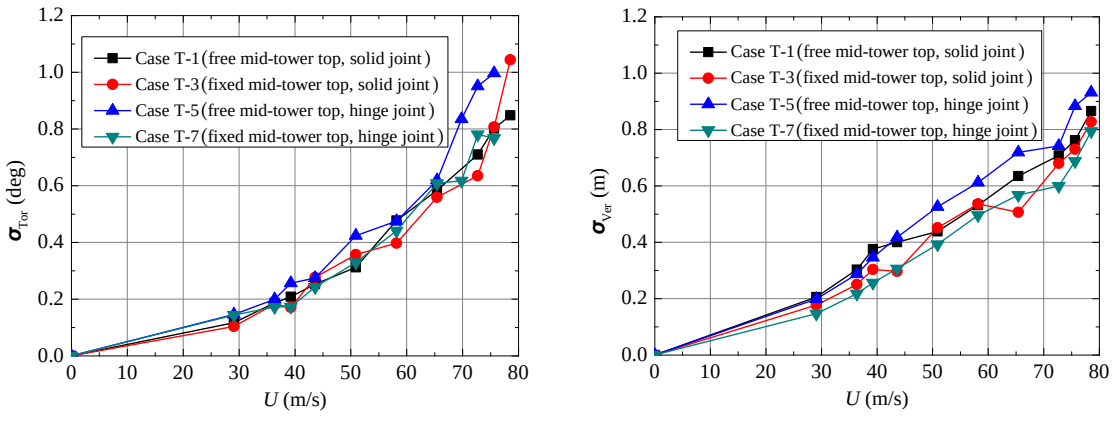

(a) torsional (b) vertical

Fig. 26 Standard deviations of responses to turbulent wind at deck midspan (w/o WD)

The test curves of the torsional and vertical standard deviations (σ_{Tor}, σ_{Ver}) vs. mean wind speed (U), for the deck responses at midspan in testing cases T-1, T-3, T-5 and T-7, to turbulent wind are shown in Fig. 26, where, the responses and wind speed have also been transferred to the prototype values. As can be seen from Fig. 26, every curve is close to others. It is indicated that mid-tower stiffness and deck supporting condition have little effect on buffeting performance of the Maanshan Bridge.

9. Conclusions

As a new long-span suspension bridge with double main spans and a typical closed streamline cross-section of single box deck, the flutter and buffeting performances of the Maanshan Bridge over Yangtze River were investigated via aeroelastic full-bridge model tests. The following major conclusions can thus be drawn according to the results of wind tunnel tests:

(1) The Maanshan Bridge has enough aerodynamic stability in both the smooth wind field and the turbulent wind field of boundary layer. The flutter pattern in smooth flow shows strong coupling behavior between vertical and torsional vibrations. Flutter dominant mode is the first symmetric torsional mode (S-T-1), which is the second torsional vibration mode in natural mode list.

(2) In smooth flow, flutter critical wind speeds, with wind deflector, are remarkably lower than those without. The flutter dominant mode, without wind deflector, is the first symmetric torsional mode (S-T-1), while that, with wind deflector, is the first antisymmetric torsional mode (A-T-1).

(3) In turbulent wind, torsional and vertical standard deviations for the deck responses at midspan in testing cases without wind deflector are generally less than those at the midspan exposed to wind in testing cases with wind deflector, respectively. The buffeting results indicate that, when double main spans of the Maanshan Bridge are exposed to wind, the existence of either span is a mass damper to the other.

(4) In turbulent wind, the fundamental modes of deck vertical bending, and torsional vibrations provides the major contributions to the buffeting responses of the Maanshan Bridge, although several higher modes also exerted a little effect on the responses. Resonant component is dominant in the buffeting response, and the contribution of the background component is very small.

(5) Both effects of mid-tower stiffness and deck supporting condition at the middle tower on the flutter and buffeting performances of the Maanshan Bridge are unremarkable.

Acknowledgements

The work described in this paper is supported by the NSFC under the Grant 51678148, and a project supported by the Natural Science Foundation of Jiangsu Province (Grant No. BK2012344), which are gratefully acknowledged.

References

Boonyapinyo, V., Lauhatanon, Y. and Lukkunaprasit, P. (2006), "Nonlinear aerostatic stability analysis of suspension bridges", *Eng. Struct.*, **28**(5), 793-803.

Chen, X.Z., Kareem, A. and Matsumoto, M. (2001), "Multimode coupled flutter and buffeting analysis of long span bridges", *J. Wind Eng. Indust. Aerodyn.*, **89**(7), 649-664.
Davenport, A.G. (1962), "Buffeting of a suspension bridge by storm winds", *J. Struct. Eng*., ASCE, **88**(6), 233-264.
Ge, Y.J. and Tanaka, H., (2000), "Aerodynamic flutter analysis of cable-supported bridges by multi-mode and full-mode approaches", *J. Wind Eng. Indust. Aerodyn.*, **86**(2), 123-153.
Ge, Y.J. and Xiang, H.F., (2011), "Extension of bridging capacity of cable-supported bridges using double main spans or twin parallel decks solutions", *Struct. Infrastruct. Eng*., **7**(7-8), 551-567.
Ge, Y.J. and Zhou, Z.Y. (2008), "Wind-resistant research on the Maanshan Bridge over the Yangtze Rover: full-model wind tunnel test", State Key Lab for Disaster Reduction in Civil Engineering, Tongji University.
Katsuchi, H., Jones, N.P. and Scanlan, R.H. (1999), "Multimode coupled flutter and buffeting analysis of the Akashi-Kaikyo bridge", *J. Struct. Eng*., ASCE, **125**(1), 60-70.
Larsen, S.V. and Larsen, A. (2003), "Wind-tunnel tests with the Chacao double suspension bridge", *Proceedings of the 11th international conference on wind engineering*, Lubbock, TX, USA.
Lin, Y.K. (1979), "Motion of suspension bridges in turbulent winds", *J. Eng. Mech*., ASCE, **105**(6), 921-932.
Thorbek, L.T. and Hansen, S.O. (1998), "Coupled buffeting response of suspension bridges", *J. Wind Eng. Indust. Aerodyn.*, **74-76**, 836-847.
Xu, Y.L., Sun, D.K., Ko, J.M. and Lin, J.H. (2000), "Fully coupled buffeting analysis of Tsing Ma suspension bridge", *J. Wind Eng. Indust. Aerodyn.*, **85**(1), 97-117.
Scanlan, R.H. and Gade, R.H. (1997), "Motion of suspended bridge spans under gusty wind", *J. Struct. Eng*., ASCE, **103**(9), 1867-1883.
Xiang, H.F. (1996), Chinese guideline for wind-resistant design of highway bridges, China Communications Press, Beijing, China. (in Chinese)
Yamada, H. and Katsuchi, H. (2005), "Study on flutter characteristics of 4-span suspension bridge", *Proceedings of the Fourth European & African Conference on Wind Engineering*, Prague, Czech Republic.
Yoshida, O. Okuda, M. and Moriya, T. (2004), "Structural characteristics and applicability of four-span suspension bridge", *J. Bridge Eng*., ASCE, **9**(5), 453-463.
Zhang, W.M. and Ge, Y.J. (2014), "Flutter mode transition of a double-main-span suspension bridge in full aeroelastic model testing", *J. Bridge Eng*., ASCE, **19**(7), 06014004.
Zhang, W.M. and Ge, Y.J. and Levitan, M.L. (2011), "Aerodynamic flutter analysis of a new suspension bridge with double main spans", *Wind Struct.*, **14**(3), 187-208.
Zhang, W.M., Ge, Y.J. and Levitan, M.L. (2013), "Nonlinear aerostatic stability analysis of new suspension bridges with multiple main spans", *J. Brazil. Soc. Mech. Sci. Eng.*, **35**(2), 143-151.
Zhang, X.J. (2008), "Wind stability of three-tower suspension bridges", *Wind Struct.*, **11**(4), 341-344.
Zhang, X.J. (2010), "Study of structural parameters on the aerodynamic stability of three-tower suspension bridge", *Wind Struct.*, **13**(5), 471-485.
Zhu, L.D., Wang, M., Wang, D.L., Guo, Z.S. and Cao, F.C. (2007), "Flutter and buffeting performances of Third Nanjing Bridge over Yangtze River under yaw wind via aeroelastic model test", *J. Wind Eng. Indust. Aerodyn.*, **95**(9), 1579-1606.

CC